International Journal of Innovative
Computing, Information and Control
Volume **9**, Number **5**, May **2013**

ICIC International ©2013 ISSN 1349-4198
pp. 1899–1917

VERSATILE LANE DEPARTURE WARNING USING 3D VISUAL GEOMETRY

Din-Chang Tseng* and Chun-Wei Lin

Institute of Computer Science and Information Engineering
National Central University
No. 300, Jhongda Rd., Jhongli 32001, Taiwan
*Corresponding author: tsengdc@ip.csie.ncu.edu.tw; gelionlin@gmail.com

Received February 2012; revised June 2012

Abstract. *This paper presents a versatile lane departure warning (LDW) system based on three-dimensional (3D) visual geometry that would help drivers avoid unintended departure from their lane during land vehicle driving. A horizontal gradient map was first calculated by an edge operator combined with the properties of lateral inhibition and far-near adaptation so that the operation would be less influenced by bad weather conditions. The lane marks were then detected with the proposed conjugate Gaussian model on the non-thresholded gradient map to make the detection more stable and less influenced by shadow boundary, windshield wipers, and the partial occlusion of other vehicles. The detected lane marks were then verified by the 3D geometric constraints of the parallel lines on the road surface to avoid the wrong detection of non-lane marks; moreover, the constraints were also used to find the other-side lane mark from the extracted one if only one lane mark was extracted on low-quality road surfaces. This means that the lane can be detected even if only one lane mark is detected. Lastly, the lane departure distance was accurately calculated from the 3D geometry of the lane marks rather than roughly estimated from the two-dimensional relationship of the lane marks on images. Overall, the properties of the proposed system are special and unique and are not present in existing systems. Based on various images of weather conditions and road surface situations, this paper demonstrates the effect and efficiency of the proposed system and compares it with other existing systems.*

Keywords: Lane-mark detection, Lane departure warning, Driving assistance, Advanced safety vehicle, Computer vision

1. **Introduction.** According to the Fatality Analysis Reporting System's Encyclopedia of National Highway Traffic Safety Administration [1], the number of fatalities caused by lane and road departure reached 12,164 in the United States in 2008. Although this number was reduced in 2009, there were still 7,696 deaths caused by departure accidents. To prevent these fatalities, lane departure warning (LDW) systems have been proposed to protect drivers from departure accidents. A standard LDW system includes two major parts: lane-mark detection and departure measurement. The lane-mark detection extracts lane marks, and then the measurement module acquires the lateral offset of the vehicle to adaptively prevent the lane departure. The lane-mark detection is not only an essential task for LDW systems, but also an important function for other vehicle warning systems. For example, vision-based forward collision and driving behavior detection systems are also generally based on lane-mark detection results.

Extensive studies have been proposed for LDW systems. The lane marks in images are tilted by perspective projection. To eliminate this tilted effect, several researchers have applied inverse perspective projection (IPM) in the preprocessing stage. Bertozzi and Broggi [2,3] proposed the Generic Obstacle and Lane Detection (GOLD) system, which

removed the perspective effect of stereo images by transforming them into a top view. Shu and Tan [4] used three parameters to describe curved lane marks in inverse perspective mapped images. They then applied a particle filter to estimate the likelihood between the lane marks drawn by the three parameters and the lane-mark edge images.

The IPM process eliminated the perspective effect of lane marks, but it required a lot of processing time. To avoid applying the time-consuming IPM, Park *et al.* [5] detected lane curve by using a lane-curve function (LCF), which was obtained by transforming the defined parabolic function on world coordinates to the image coordinates. Li *et al.* [6] applied a Sobel operator on multi-resolution gray-level images to obtain edge images and then applied a very low threshold to filter the edges with low response. Finally, the three-dimensional (3D) lane model was reduced to two-dimensional (2D) circular arcs, and the arcs were determined by a multi-resolution fitting method. Jung and Kelber [7] proposed an LDW system based on the linear-parabolic model, where lane marks were extracted by an edge distribution function and a modified Hough transform. Zhou *et al.* [8] used a deformable template to model lane marks in the gradient map. They then applied the Tabu algorithm to detect the lane marks based on a likelihood function that fit the edge-point positions and directions with the lane model. Based on the lane detection result, a particle filter was then used to help estimate the lane shape in the consecutive images. Hsiao *et al.* [9] designed an embedded ARM-based LDW system. The edge responses were extracted by a one-dimensional Gaussian smoother and a global edge detector. Peaks in every scan line were detected by the peak-finding algorithm. Finally, all detected peaks were combined to fit a line segment to represent a lane mark.

Chang *et al.* [10,11] extracted the maximum gray-level gradient on every horizontal scanning line to obtain the dotted lane marks. Then, straight-line equations of lane marks were estimated based on the starting point and terminal point of the longest continuous lines. Chen *et al.* [12] utilized the dark-light-dark (DLD) characteristic of the intensity to extract lane-mark candidates. The distance between the dark-light and light-dark transmissions of each lane-mark candidate was estimated. Then, a least-square approximation was used to obtain the lane mark information by those candidates in which the distance between two transmissions exceeded a predefined threshold. In addition, several commercial LDW products developed by AssistWare Technology, Inc. [13-15], Iteris, Inc. [13-15], Mobileye, Inc. [13-16], Continental AG [14], etc., are currently on the market.

In most of these studies and products, the lanes are only detected by utilizing the extreme edge response on one or two sides of a lane mark without considering the relationship between the two edge responses and a correlation between the two lane marks of a lane. In such an outdoor application, if a lane detector does not use extra information or apply special treatment, the detector will easily encounter the following problems: (*i*) it will be sensitive to the bad weather conditions, (*ii*) the results will be unstable for the low-quality lane marks and road surface, and (*iii*) it might interpret a non-lane mark as a lane mark. A usable LDW system should be stable in various weather conditions and for various lane-mark types, even when the quality of the lane marks is low. Furthermore, the system should reduce the interpretation of non-lane marks as lane marks and should minimize the calibration procedure of the camera position.

In this study, we propose a versatile LDW system based on 3D visual geometry to achieve the above-mentioned goals. To reduce the influence of bad weather conditions, edge pixels were extracted by an edge detector combined with the facilities of lateral inhibition of a human visual system and far-near adaptation. Then the lane marks were detected by the proposed conjugate Gaussian model based on the extracted edges to make the detection more stable and less influenced by shadow boundary, windshield wipers, and the partial occlusion of other vehicles. In a few stubborn cases, the above detection still

failed; thus, the detected lane marks needed to be verified by the geometric constraints of the parallel lane marks on the road surfaces. These constraints included the relationship between the angle and intercept of a line and the known 3D lane width.

Sometimes, the condition of the road was poor due to a lack of maintenance; in these cases, the partial lane marks were nearly invisible and were hard to detect. In such cases, the geometric constraints were also used to find the other-side lane mark from the extracted one if only one lane mark was extracted. Finally, the lane departure distance was accurately calculated from the 3D geometry of the lane marks, rather than roughly estimated from the 2D relationship of the lane marks on the images. Moreover, the proposed system needed no calibration of camera orientation. All of these properties of the proposed system are special and unique, and have not been utilized by the existing systems and products currently on the market. Based on various images of weather and road surface conditions, this paper will demonstrate the effect and efficiency of the proposed system and compare it to the other systems.

The remaining sections of the paper are organized as follows. In Section 2, we present the lane-mark detection with the properties of the lateral inhibition, the far-near adaptation, and the conjugate Gaussian model. In Section 3, we propose geometric constraints for verification of the detected lane marks and for correcting possible wrong detection. We describe the determination of lane departure in Section 4, and in Section 5, we report and compare the experimental results. The conclusion is given in Section 6.

2. **Lane-Mark Detection.**

The proposed lane-mark detector was constructed based on the property of the human-vision lateral inhibition, the far-near adaptation, and the conjugate Gaussian model.

2.1. **The lateral inhibition property.**

Lateral inhibition [17] is one property of the human visual system that can be used to enhance the responses of edges between lane marks and the road surface. Thus, it is especially helpful for detection in bad weather conditions.

In all situations, lane marks in the images tended to be vertical, so a vertical-edge detector was sufficient to detect all lane marks. Assume the gray levels of pixels p_0, p_1, p_2, $\ldots$, p_n in an image row were f_0, f_1, f_2, $\ldots$, f_n. The horizontal first difference $e_{1,i}$ for p_i was defined as

$$e_{1,i} = f_{i+1} - f_i, \tag{1}$$

and the horizontal second difference $e_{2,i}$ for p_i was defined as

$$e_{2,i} = f_{i+1} - f_{i-1}. \tag{2}$$

In general, the outdoor images were more or less blurred. To use the edge detection to improve these kinds of images, we adopted the second-difference edge detector. With the effect of lateral inhibition, f_i was perceived as $f_i - \alpha f_{i-1} - \alpha f_{i+1}$, where α was the inhibition factor and generally set at about 20%. The second and third terms αf_{i-1} and αf_{i+1} were just the neighboring inhibition to pixel p_i. Thus, the edge response for p_i became

$$\begin{aligned} e'_{2,i} &= (f_{i+1} - \alpha f_i - \alpha f_{i+2}) - (f_{i-1} - \alpha f_{i-2} - \alpha f_i) \\ &= \alpha f_{i-2} - f_{i-1} + f_{i+1} - \alpha f_{i+2}. \end{aligned} \tag{3}$$

$e'_{2,i}$ had a higher contrast than $e_{2,i}$; thus, $e'_{2,i}$ was more stable for edge detection in bad weather conditions.

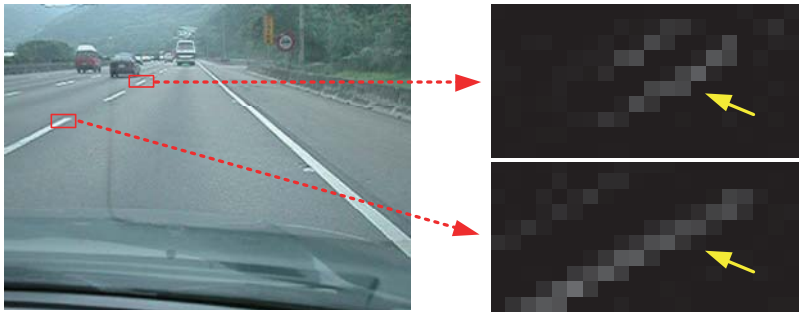

FIGURE 1. The different edge responses for different-distanced lane marks. The average of edge responses is 57.5 for far lane mark and 69.8 for near lane mark.

2.2. **Adjustment of far-near edge weights.** Due to the effect of perspective projection, far lane marks are smaller and more blurred than near lane marks in images. The edge response of a near lane mark is therefore stronger than that of a far lane mark, as shown in Figure 1. This means that the direction of a linear lane model is dominated by the near lane mark. However, the far lane marks provide more directional information than the near lane marks provide for lane cruise driving. Thus, we needed to balance the weights of far and near lane mark edges. Our adjustment of the edge responses was based on the vertical coordinate of the images. For a pixel p at coordinates (x, y) with edge strength e, the adjustment of e was defined as

$$e' = e\left(\beta \frac{y - y_{\min}}{y_{\max} - y_{\min}} + 1\right), \tag{4}$$

where β was the adjustment factor, $\beta > 0$, and $y_{\max}$ and $y_{\min}$ were the upper and lower bounds of the considered vertical range for detecting lane marks in images, respectively. The adjustment of far and near edge responses made the lane cruise driving on curved lanes more stable.

2.3. **Lane detection by the conjugate Gaussian model.** To detect the real lane marks, we extracted both the left and right borders of a lane mark in the horizontal second-difference map simultaneously. The lane border was defined as

$$y = \tan\theta(x - b), \tag{5}$$

where θ was the angle between the lane border and x axis (horizontal), $\tan\theta$ was called the slope, and b was the intercept between the lane border and the x axis.

Without thresholding, we accumulated the edge responses of pixels along every lane border specified by θ and b to construct an accumulating difference map on the $\theta - b$ parameter space. Then, from the accumulating difference map, we found the maximum and minimum pair as shown in Figure 2. In Figure 2(b), the horizontal plane represents the intercept in pixels and the angle in degrees, and the vertical axis is the accumulation of edge responses corresponding to the angle and intercept. The highest peak denotes the highest potential of the left border of a lane mark, and the lowest valley denotes the highest potential of the right border of the same lane mark.

In general, the shape of the peak and valley in the accumulating difference map was like a pair of asymmetric Gaussian functions. We defined a conjugate Gaussian model to match the peak and valley in the map as shown in Figure 3. The zero-mean bivariate

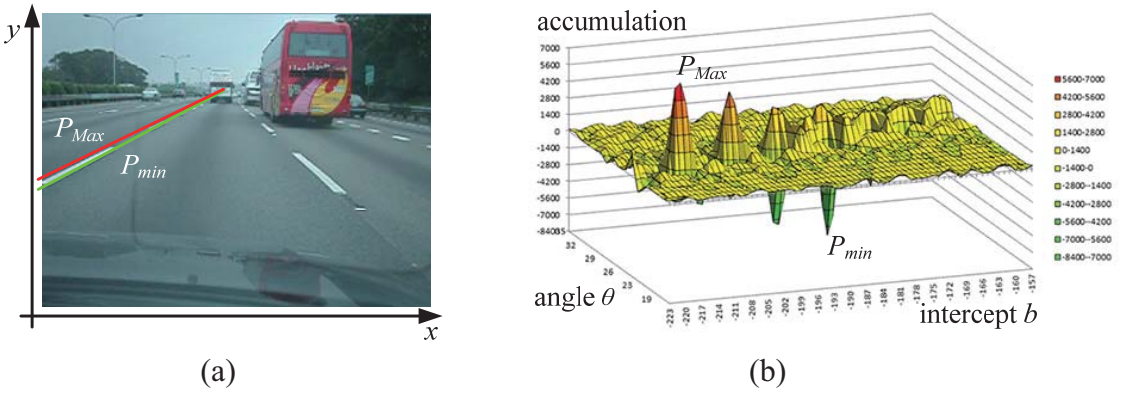

FIGURE 2. The accumulating difference map on the $\theta - b$ parameter space. (a) Two lane borders of a left dashed lane mark. (b) The highest peak P_{Max} and the deepest valley $P_{\min}$ present the left and right borders of the left lane mark, respectively.

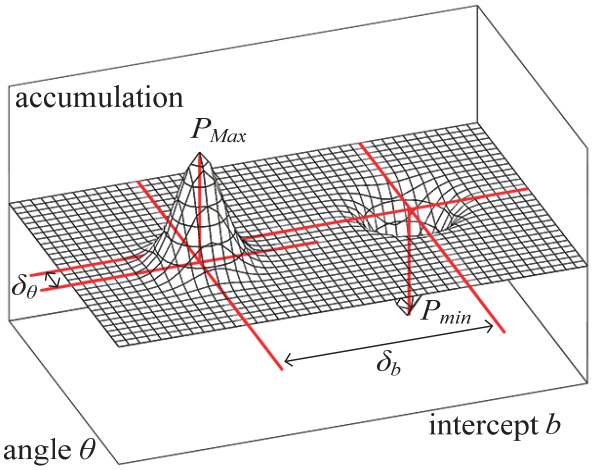

FIGURE 3. The conjugate Gaussian model

Gaussian function is shown as

$$G(x_1, x_2) = \frac{1}{2\pi\sigma_{11}\sigma_{22}\sqrt{(1-{\rho_{12}}^2)}} e^{\frac{-1}{2(1-{\rho_{12}}^2)}\left\{\left(\frac{x_1}{\sigma_{11}}\right)^2+\left(\frac{x_2}{\sigma_{22}}\right)^2-2\rho_{12}\frac{x_1}{\sigma_{11}}\frac{x_2}{\sigma_{22}}\right\}}, \tag{6}$$

with $\rho_{12} = \frac{\sigma_{12}}{\sqrt{\sigma_{11}}\sqrt{\sigma_{22}}}$ for variables x_1 and x_2; this was used to define the proposed conjugate Gaussian model. However, the model was too complicated to be efficient. We assumed that (i) the two variables were independent and that (ii) the variances of the two variables were the same as σ^2 to simplify the bivariate Gaussian function as

$$G(x_1, x_2) = \frac{1}{2\pi\sigma^2} e^{-\frac{{x_1}^2+{x_2}^2}{2\sigma^2}}. \tag{7}$$

A conjugate Gaussian model was coupled with a positive Gaussian function G_P and a negative Gaussian function G_N in the $\theta - b$ space, where G_P and G_N were defined as

$$G_P = G(b, \theta) = \frac{1}{2\pi\sigma^2} e^{-\frac{b^2+\theta^2}{2\sigma^2}} \tag{8}$$

and

$$G_N = -G(b,\theta) = -\frac{1}{2\pi\sigma^2} e^{-\frac{b^2+\theta^2}{2\sigma^2}}. \tag{9}$$

Two borders of a lane mark in the images have a specified relationship. We defined the Gaussian functions in the conjugate Gaussian model to have a similar relationship. We searched the lane borders in the accumulating difference map using the criterion

$$(b',\theta') = \arg\max_{b,\theta} \left[E_P(b,\theta) + E_N(b,\theta)\right], \tag{10}$$

with two fitness functions

$$E_P(b,\theta) = \frac{\sum_{m=-i}^{i}\sum_{n=-j}^{j} G(m,n)E(b+m,\theta+n)}{\sqrt{\sum_{m=-i}^{i}\sum_{n=-j}^{j}[G(m,n)]^2 \sum_{m=-i}^{i}\sum_{n=-j}^{j}[E(b+m,\theta+n)]^2}} \tag{11}$$

and

$$E_N(b,\theta) = \frac{-\sum_{m=-i}^{i}\sum_{n=-j}^{j} G(m,n)E((b+\delta_b)+m,(\theta+\delta_\theta)+n)}{\sqrt{\sum_{m=-i}^{i}\sum_{n=-j}^{j}[G(m,n)]^2 \sum_{m=-i}^{i}\sum_{n=-j}^{j}[E((b+\delta_b)+m,(\theta+\delta_\theta)+n)]^2}} \tag{12}$$

where E was the accumulating difference map and δ_b and δ_θ were the relative locations of the peak and valley in the intercept axis and angle axis, respectively. E_P and E_N were correlations of the G_P and G_N functions with the accumulating difference map, respectively. A lane mark was detected if its function value $E_P(b',\theta') + E_N(b',\theta')$ was greater than threshold value T_l.

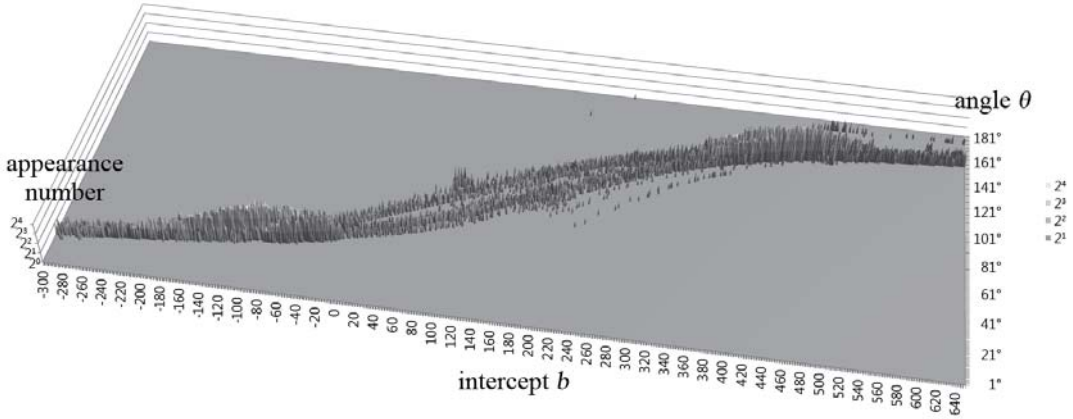

FIGURE 4. Analysis of intercepts and slope angles of the used lane model. The map base represents intercept and slope angle of lane models. The height is the accumulation of the detected lane marks. The distribution presents the relationship between intercepts and angles of correct lane marks.

The intercept b and slope angle θ of the lane model were dependent. To reduce the search space for finding lane borders by Equation (10), we analyzed all possible relationships between the intercept and slope angle of the lane model to construct an intercept-angle relationship map as shown in Figure 4. The map was built by analyzing 27,312 frames with 54,624 lane marks. In the map base, the two axes represented the intercept and slope angle, respectively. The height represented the appearance number of detected lane marks with the corresponding intercepts and slope angles. Based on the statistical data, we utilized a Gaussian function,

$$G(\theta) = \frac{1}{\sqrt{2\pi\sigma^2}} e^{-\frac{(\theta-\bar{\theta}_i)^2}{2\sigma^2}}, \tag{13}$$

to describe the corresponding angles for each intercept, where $\bar{\theta}_i$ was the mean of slope angles corresponding to the intercept b_i. We then built a look-up table to record the Gaussian mean $\bar{\theta}_i$, standard deviation σ_i, and the upper/lower bounds of the slope angles indexing by the intercept b_i. When searching for lane borders, the upper and lower bounds improved the performance.

Moreover, the look-up table was also used for finding the relative intercept δ_b and slope angle δ_θ. In Equation (12), the δ_b and δ_θ were variants for different b and θ; b was the intercept of the left border of a lane mark. With the known lane-mark width and known relationship between the camera and the world coordinate system [18], we found the intercept b' of the right border of the lane mark on the image and then acquired $\delta_b = b' - b$. Afterward, from the above look-up table, we found the means of slope angles $\theta(b)$ and $\theta(b')$ for intercepts b and b', respectively, and then acquired $\delta_\theta = \theta(b') - \theta(b)$.

3. **Lane Verification.** With the conjugate Gaussian model, we found that we could accurately detect lane marks. However, it was still possible that some traffic signs and unexpected stripes on the road surface could be wrongly taken as lane marks, as shown in Figure 5. A robust lane detection system should possess the ability to reduce "false positive" errors; in other words, a robust system should not interpret a non-lane mark as a lane mark.

3.1. **Three-dimensional geometric verification.** We used two lane mark clues to verify whether the detected lane marks are correct or not, which are (i) the relationship between intercept b and slope angle θ of a lane model and (ii) the known 3D lane width.

3.1.1. *Judgment on the relation between intercepts and slope angles.* In Section 2.3, we stated that the intercept b and slope angle θ of a lane model are mutually dependent on images. Based on this premise, we built a look-up table to record the related data. We used the Gaussian mean $\bar{\theta}_i$ and standard deviation σ_i to verify the correctness of detected

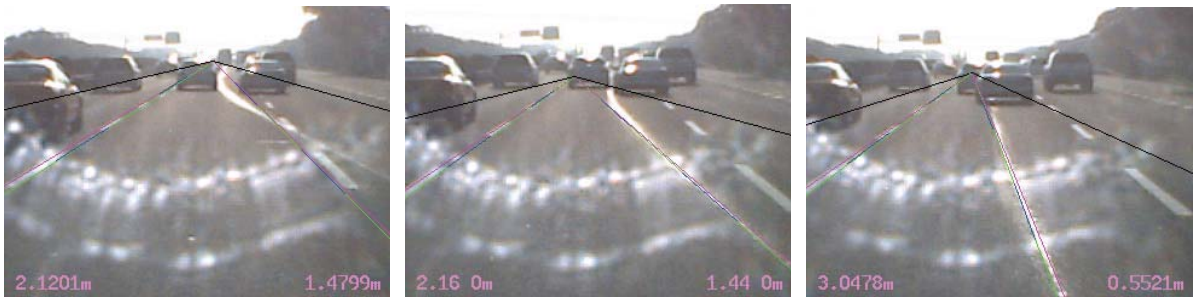

FIGURE 5. Wrong detection due to the extra liquid stripe on road surface

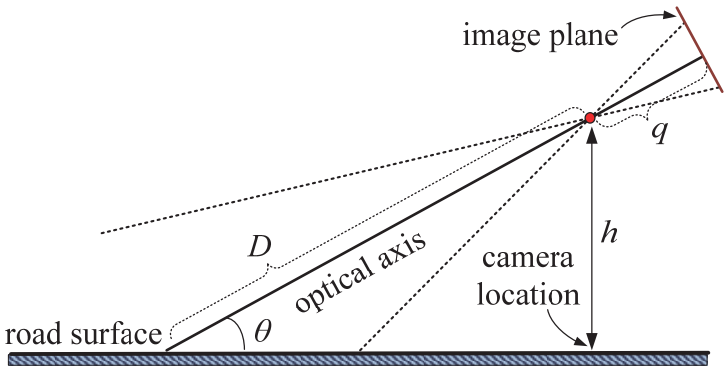

FIGURE 6. The side view of the relationship between camera and road plane

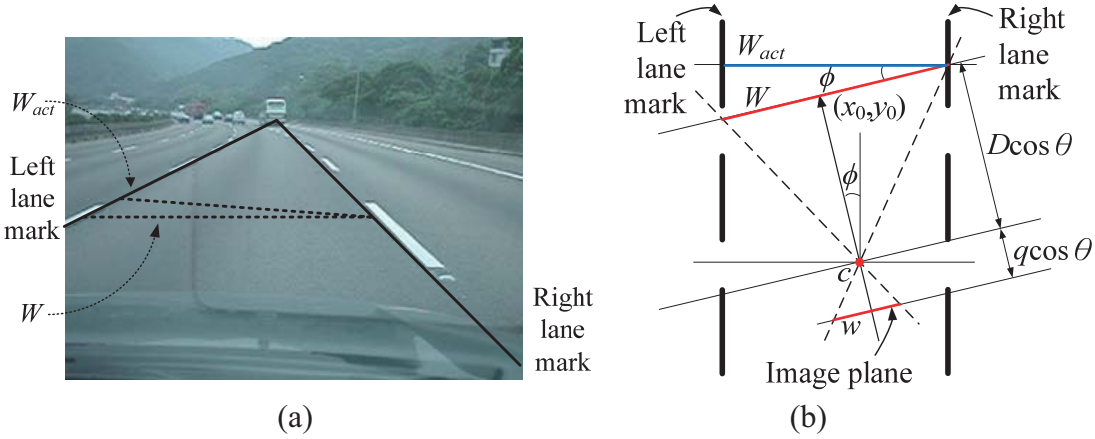

FIGURE 7. The relationship of lane marks on image plane and road plane. (a) Front view. (b) Top view.

lane mark. The angle range for each intercept was set to cover 99.7% of correct lane marks. That is, if $|\theta - \bar{\theta}_i| < 3\sigma$, then θ was accepted.

3.1.2. *Judgment on the lane width.* If we have calibrated the relative position and orientation of the camera to the world coordinate systems, we could derive the transformation formulas from a point location in the world coordinate system to that on the image. The proposed system verified whether or not the detected lane marks were correct by projecting the known lane width onto the image to compare it with the detected lane width on the image.

We utilized the monocular computer vision method proposed by Tseng [18] to estimate yaw angle ϕ and pitch angle θ of the 3D lane marks with respect to the camera coordinate system. As shown in Figure 6, the height of the camera was h and the distance D from the intersection point of the camera optical axis and the road surface to the camera was

$$D = \frac{h}{\sin\theta}. \tag{14}$$

As shown in Figure 7(b), if the camera had no roll rotation to the road surface, the visual lane width W on the road surface at $D\cos\theta$ distance from the camera had the relation of

$$\frac{W}{D} = \frac{w}{q}, \tag{15}$$

where w was the lane width at the image center and q was the distance from the camera lens center to the image plane. If the vehicle had yaw rotation of angle ϕ with respect to the road surface normal, the actual lane width W_{act} and the visual lane width W had the relation $W_{act} = W \cos\phi$. Then,

$$w = \frac{q}{D}W = \frac{q\sin\theta}{h}W = \frac{q\sin\theta}{h}\frac{W_{act}}{\cos\phi}. \tag{16}$$

Actually, for any vertical location y in the image, we could derive the relationship between the lane widths on the road surface and on the image as

$$w(y) = \frac{W_{act}}{h\cos\phi}\left(q\sin\theta - (y - y_c)\cos\theta\right), \tag{17}$$

where y_c was the vertical coordinate of the image center.

3.2. **The rectification of wrong detection.** If the angle and intercept parameters of a lane model were not compatible or the lane width did not match the known width, we could search a more correct lane mark pair from one detected lane mark and the known lane width. We categorized this rectification into two cases: (i) only one lane mark was extracted or (ii) both lane marks were extracted but the lane width was not correct.

If only one lane mark was extracted, we utilized the lane mark to infer the other based on the 3D geometry of two lane marks and the known lane width. As described in Section 3.1.2, we chose any two different vertical locations y_1 and y_2 to compute $w(y_1)$ and $w(y_2)$ from Equation (17); we then inferred two horizontal locations x_1 and x_2 from $w(y_1)$, $w(y_2)$ and the extracted lane mark. The line passing through (x_1, y_1) and (x_2, y_2) just specify the desired lane mark. In the above process, one of (x_1, y_1) and (x_2, y_2) could be replaced by the pre-acquired vanishing point of the lane marks [19].

In the case of wrong lane width, we assumed that one of the detected lane marks was correct, but that we did not know which one. Hence, we used the previous method from the detected left lane mark to find the corresponding right one and the detected right lane mark to find the corresponding left one. Then we used the fitness functions of Equations (11) and (12) to judge which pair of lane marks was the better one. The pair with the larger fitness function value was chosen as the desired lane marks. An example of the rectification is shown in Figure 8.

4. **Lateral Offset Determination.** The lateral offset estimation method was first proposed by Tseng [18], and we modified the decision criterion for departure. The proposed method was based on 3D perspective geometry to estimate the lateral offset of the host vehicle from the detected lane marks. We assumed that there were only pan and tilt rotations of the camera to the road surface (world coordinate system); hence, the driving situation is shown in Figure 9. Figure 9(a) shows a top view of a camera in a lane. The camera is located at c and has a pan angle ϕ to left. L and R are the distances from c to the left and right lane marks, respectively. Figure 9(b) is the corresponding front-view image, where two lane marks are perspective projected onto the image to intersect a vanishing point v. l and r are the distances from the midpoint of the image's lower border to the left and right lane marks along the horizontal direction. These l and r are just the l and r shown in Figure 9(a).

In Figure 9(b), the line $\bar{vc}$ is called the vehicle location line that passes c and is parallel to the lane marks. Based on the principle of the same triangles, the ratio of the distances from c to the left and the right lane marks in the image is the same as that in the 3D space; that is, l/r is equal to L/R. If the lane width was fixed and known, then the actual

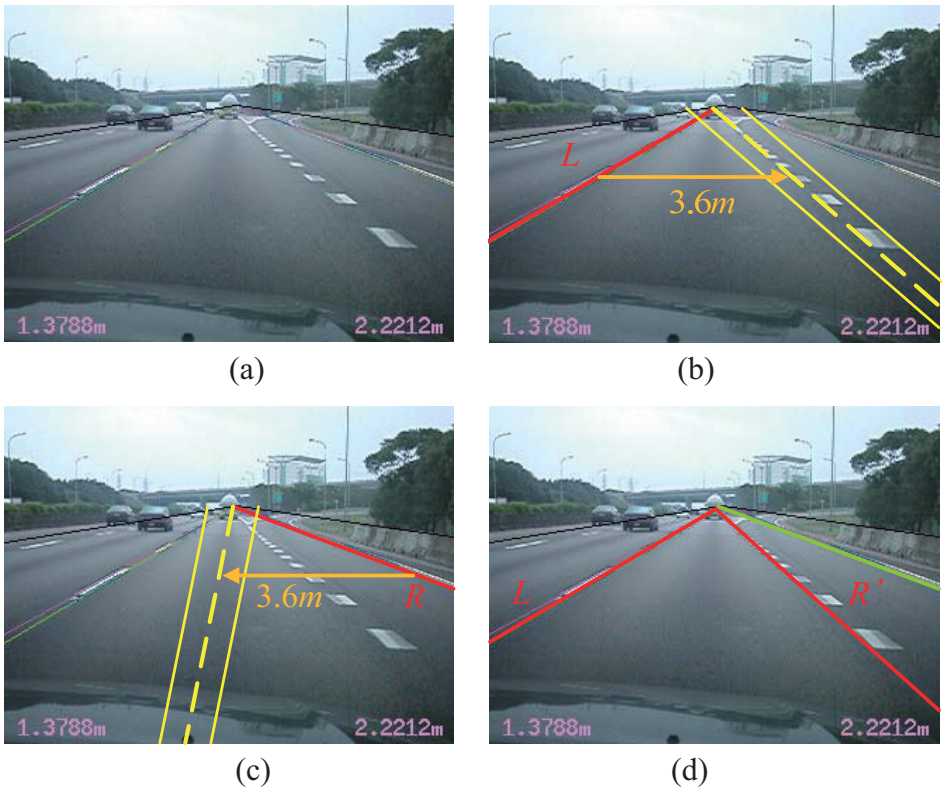

FIGURE 8. Steps of rectification for wrong lane marks. (a) The wrong detected right lane mark. (b) (c) From one detected lane mark to find the other one. (d) Choosing the better one.

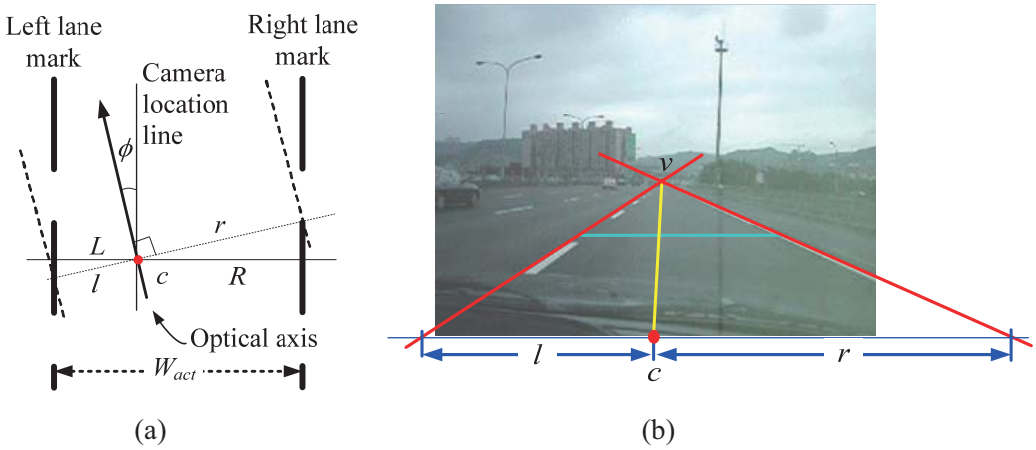

FIGURE 9. A camera in a lane. (a) Top-view diagram. (b) The front-view image.

distances from the camera to both lane marks could be calculated by

$$L = \frac{l}{l+r} W_{act} \tag{18}$$

and

$$R = \frac{r}{l+r} W_{act}, \tag{19}$$

where W_{act} was the actual lane width.

A simple warning for lane departure was set as follows. If the vehicle width was W_v, the camera was set behind the windshield with distances D_l and D_r to the vehicle left and right borders, respectively. Then the warning would be raised if the distance from the vehicle border to the lane mark was less than T_t. That is,

$$\begin{cases} \text{If } L - D_l < T_t, & \text{the vehicle is unintentionally departing to the left side,} \\ \text{If } R - D_r < T_t, & \text{the vehicle is unintentionally departing to the right side.} \end{cases} \tag{20}$$

5. **Experiments.** The proposed LDW system was tested with many images captured in various weather conditions and road surface situations such as heavy rain, glare from the sun, cast shadows, light noise, night, and double-lane marks, as shown in Figures 5, 8 and 10. The performance of most LDW systems is generally influenced by these conditions and situations. We also compared the proposed method with the other existing methods. All experimental images were 320×240 pixels. The proposed system was examined on PC-based platforms, Apple iPhone systems, and Android-based mobile phones.

5.1. **Effect of lateral inhibition.** Both synthetic and real images were examined for the effects of lateral inhibition. The results of the first-difference and second-difference vertical edge detections and edge detections with and without lateral inhibition were compared.

FIGURE 10. Image samples with various weather conditions and road-surface situations. (a) (b) Heavy rain. (c) (d) Glare from the sun. (e) (f) Cast shadow. (g) Light noise. (h) Night. (i) Double lane marks.

TABLE 1. Effects of lateral inhibition

Experimental video	Number of lane marks	Lateral inhibition	Detected marker	Detection rate
Sunny day on highway	2,436	With	2,395	98.3%
		Without	2,379	97.8%
Sunny day at exit of highway	2,054	With	2,024	98.5%
		Without	1,980	96.4%
Sunny day in downtown	1,398	With	1,358	97.1%
		Without	1,342	96.0%
Cloudy day at exit of highway	576	With	572	99.3%
		Without	566	98.3%
Rainy day on ramp of highway	1,902	With	1,867	98.2%
		Without	1,835	96.5%

One artificial 320 × 240 image with ideal lane marks is shown in Figure 11(a). The first-difference edge detection without lateral inhibition generated a low-contrast edge response (accumulation) as shown in Figure 11(b); with the lateral inhibition, the contrast of the edge response was enhanced, as shown in Figure 11(c). The second-difference edge detector gained a more significant edge response than the first-difference edge detector, as illustrated in Figure 11(d) without lateral inhibition and Figure 11(e) with lateral inhibition. With the proposed conjugate Gaussian model, the fitness function values of the four maximum edge responses were 0.94, 0.97, 1.84 and 1.89, respectively. The second-difference edge detector with lateral inhibition had the strongest contrast in the accumulating difference map; hence, the detection was more stable. In other words, we were able to avoid extracting the wrong lane mark. This phenomenon was even more obvious in real images.

One real image is evaluated as shown in Figure 12(a). The results and comparison are given in Figures 12(b)-12(e). The complex scene has more little peaks and valleys than in the artificial image. In these complicated accumulating difference maps, it is easy to make a wrong detection. The second-difference edge detector with lateral inhibition generated the strongest contrast and was less influenced by the rugged surface, as shown in Figure 12(e); the detector generated a more stable solution. The fitness function values of these four maximum edge responses were 0.89, 0.98, 1.80 and 1.96, respectively. We compared the effects of lateral inhibition in various weather conditions as listed in Table 1. The lane detector with lateral inhibition had a higher detection rate in various weather conditions. The average detection rate was 98.21% with lateral inhibition and 96.84% without lateral inhibition.

5.2. **Effect of the conjugate Gaussian model.** The purpose of the conjugate Gaussian model was to extract lane marks without being influenced by shade, windshield wipers, and the partial occlusion of other vehicles. As one example shows in Figure 13(a), if the conjugate Gaussian model was not applied, the edge with the strongest edge response was wrongly extracted as a lane mark; the edge was actually caused by a viaduct shadow, which generated the maximum peak P'_{Max} in the accumulating difference map as shown in Figure 13(c). However, P_{Max} and $P_{\min}$ formed the best pair with the conjugate Gaussian model as shown in Figure 13(b). In this case, the fitness function value was 1.53 for the pair of P_{Max} and $P_{\min}$, but was only 0.60 for the pair of P'_{Max} and $P'_{\min}$, where $P'_{\min}$ was obtained from P'_{Max} and the estimated δ_θ and δ_b. Based on the test samples, the effect of the conjugate Gaussian model is compared and listed in Table 2. The overall detection

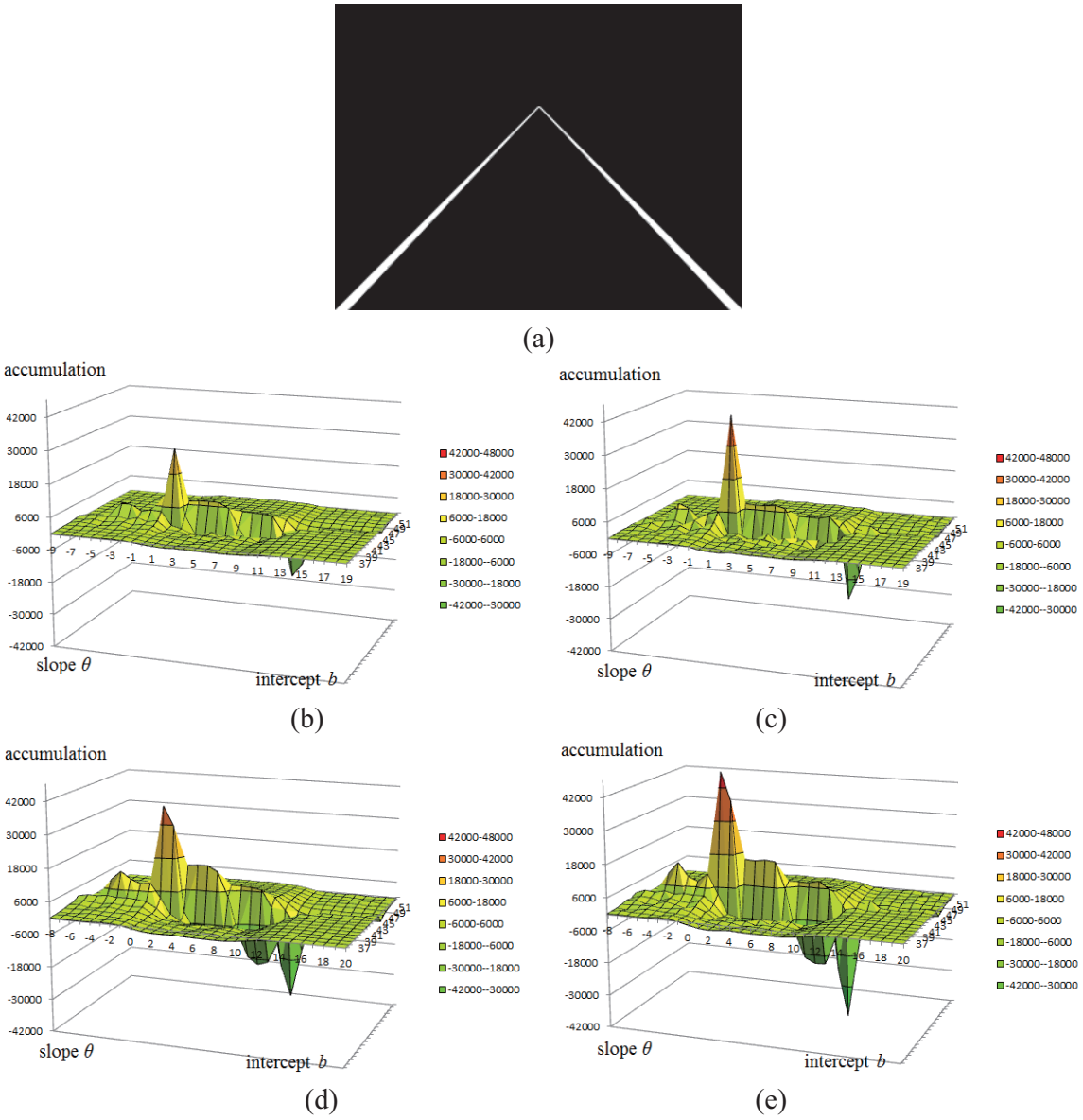

FIGURE 11. The comparison of accumulating edge responses for an artificial image. (a) The artificial 320 × 240 image. (b) The first-difference edge detector without lateral inhibition. (c) The first-difference edge detector with lateral inhibition. (d) The second-difference edge detector without lateral inhibition. (e) The second-difference edge detector with lateral inhibition.

rate of lane marks with and without the conjugate Gaussian model observably increased from 86.90% to 98.21% in the five experimental videos.

5.3. **Effect of the three-dimensional geometric constraints for lane verification.** The 3D geometric constraints included the relationship between intercepts and slope angles and the 3D lane width constraint. We took six long-period videos with 54,479 images to evaluate the first constraint. Half of the videos were used to build the intercept-angle relation map, and the other half were used to examine the map. In the examined videos, only 0.7% of lane marks failed to be detected. Most failures appeared on highway on- or off-ramps or in the situation of rapid lane changes, where the relation of intercepts

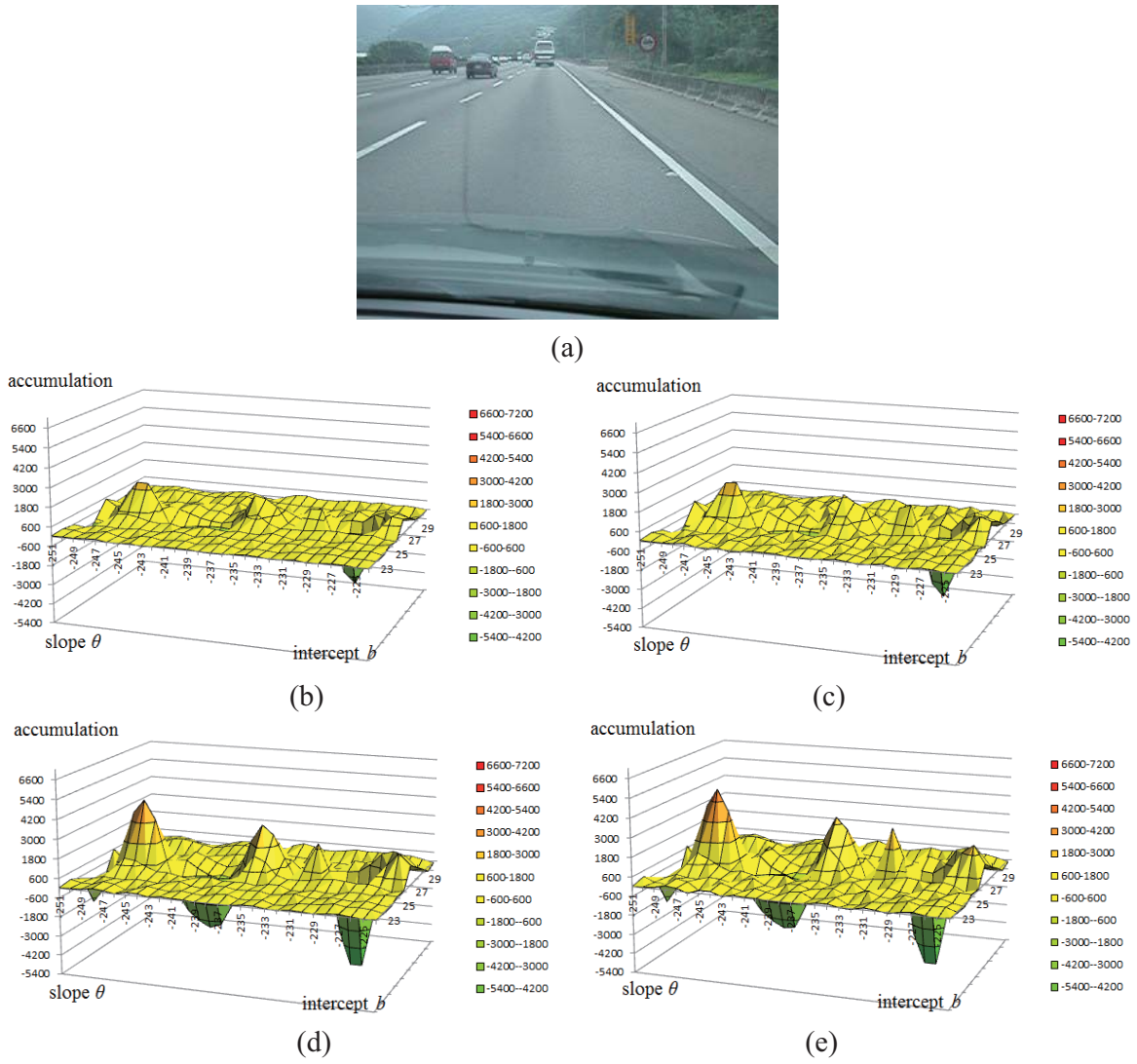

FIGURE 12. The comparison of accumulating edge responses for a real image. (a) A real image. (b) The first-difference edge detector without lateral inhibition. (c) The first-difference edge detector with lateral inhibition. (d) The second-difference edge detector without lateral inhibition. (e) The second-difference edge detector with lateral inhibition.

and slope angles was out of the range of criterion $|\theta - \bar{\theta}_i| < 3\sigma$. For the 3D lane width constraint, we took five videos containing 37,048 images to evaluate. In every image, we estimated two lane widths with different distances and then back-projected the widths onto the road surface to compare them with the actual lane width. The difference between the estimated lane width and the actual width was less than 0.09 meters on average.

5.4. **The performance of lane verification and rectification.** Two situations were used to evaluate the performance of lane verification. One was the host vehicle taking a highway exit as shown in Figure 14(a). The right solid lane mark was divided into a solid and a dashed lane mark. The solid lane mark had a larger edge response; thus, the solid lane mark was extracted. The other situation was a noticeable liquid stripe on the road surface as shown in Figure 5. The stripe had a stronger edge response than the dashed lane mark; thus, the stripe was extracted. Based on the proposed verification process, the

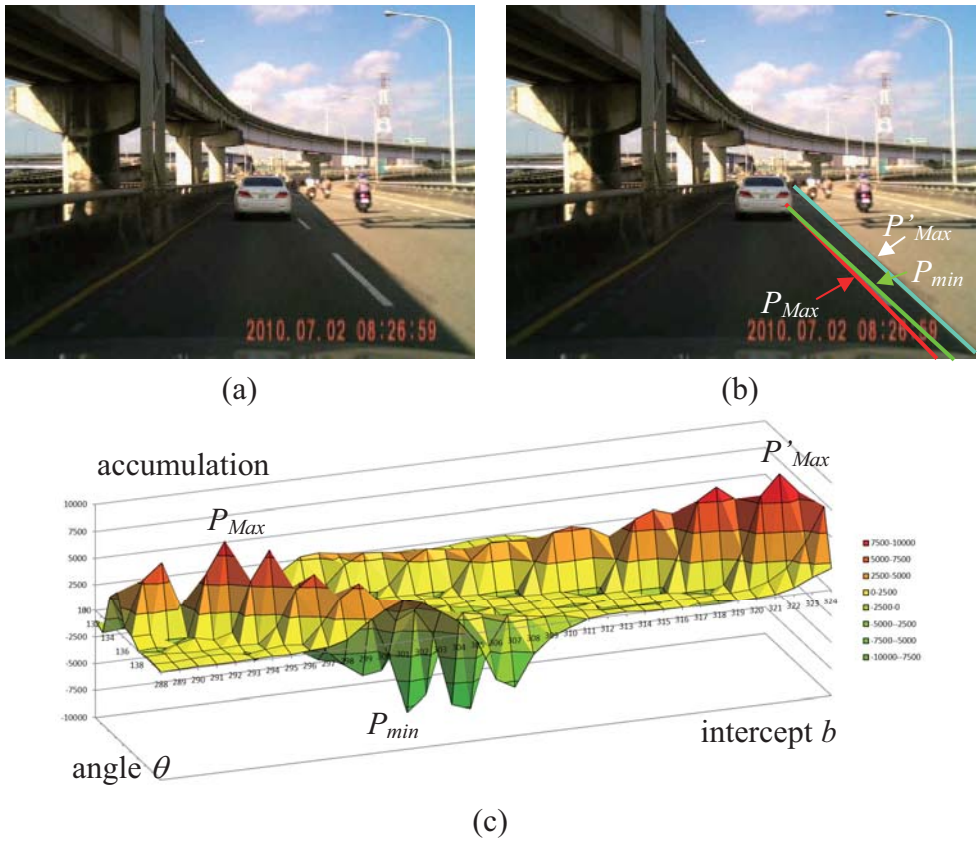

FIGURE 13. The conjugate Gaussian model for lane-mark detection. (a) The viaduct shadow leads the highest edge response on road surface. (b) The edges of peaks P_{Max}, $P_{\min}$, and P'_{Max} in accumulating difference map. (c) The accumulating difference map on the $\theta - b$ space. P'_{Max} is the global maximum, but P_{Max} and $P_{\min}$ form the best pair with the proposed conjugate Gaussian model.

TABLE 2. Effects of conjugate Gaussian model

Experimental video	Number of lane marks	Conjugate Gaussian model	Detected lane marker	Detection rate
Sunny day on highway	2,436	With	2,395	98.3%
		Without	1,971	80.9%
Sunny day at exit of highway	2,054	With	2,024	98.5%
		Without	1,959	95.4%
Sunny day in downtown	1,398	With	1,358	97.1%
		Without	1,218	87.1%
Cloudy day at exit of highway	576	With	572	99.3%
		Without	486	84.4%
Rainy day on ramp of highway	1,902	With	1,867	98.2%
		Without	1,636	86.0%

lane marks in both situations were correctly detected as shown in Figures 14(b) and 15, respectively. The detection results without and with the lane verification are compared in Table 3. The detection rate of lane marks improved 25.34% on average.

FIGURE 14. The comparison of lane detection without and with rectification process. (a) Without lane verification. (b) With lane verification.

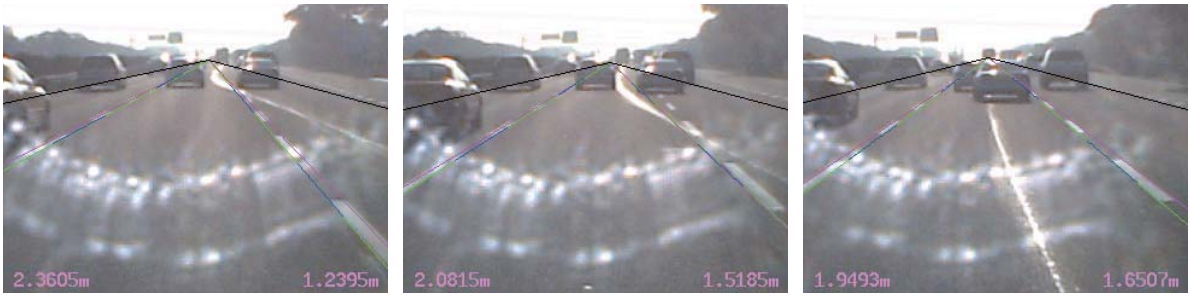

FIGURE 15. Lane marks are correctly detected from the liquid stripe

TABLE 3. Detection rate improved by the lane rectification

	Verification	# of lane marks	Detected #	Detected rate	Improvement
Situation 1	Without	342	292	85.4%	9.9%
	With	342	326	95.3%	
Situation 2	Without	700	429	61.3%	32.8%
	With	700	659	94.1%	

5.5. **Comparison of methods.** The proposed method and two existing methods were compared based on images of various weather conditions and road surface situations. The first existing method, based on line fitting of maximum gradient points on all scan lines to find lane marks, was used in [9-11]. The second existing method, based on line fitting of low-high-low gray-level patterns on every scan line to detect lane marks, was used in [12]. Twelve videos, including the cases shown in Figures 5, 8 and 10, were tested. There was a total of 22,808 images; in these images, two different tilt angles and four camera heights were used.

The detection rates of the three methods are compared and shown in Table 4. The proposed method included more features and showed the best detection rates. All cases shown in Figures 5, 8 and 10 were correctly detected by the proposed method, as shown in Figures 14(b), 15 and 16. Based on the proposed detection with lateral inhibition property, the lane marks in Figures 16(a)-16(e) were correctly detected. Based on the proposed conjugate Gaussian model, the lane marks in Figure 16(f) were correctly detected. Based on the proposed rectification process for known lane width, the invisible lane marks in Figures 16(g) and 16(h) were recovered. Based on the proposed rectification process for known lane width, the lane marks in Figures 14, 15 and 16(i) were detected. The two existing methods failed in the all cases included in Figures 15 and 16(f)-16(h). The second

FIGURE 16. The detection results of the images shown in Figure 10. (a) (b) Heavy rain. (c) (d) Glare from the sun. (e) (f) Cast shadow. (g) Light noise. (h) Night. (i) Double lane marks.

FIGURE 17. The very stubborn cases in which the lane marks are not detectable

TABLE 4. Comparison of detection rates among the proposed method and two existed methods

	# of lane marks	Detection rates		
		Fitting of maximum gradient points	Fitting of low-high-low pattern	The proposed method
Sunny day on highway	14,550	97.43%	91.30%	99.22%
Sunny day in downtown	7,262	93.14%	92.87%	98.22%
Cloudy day at exit of highway	8,026	95.13%	94.47%	96.62%
Rainy day on highway	7,274	89.47%	84.20%	99.75%
Nighttime on highway	7,264	97.80%	97.27%	99.56%
Road with liquid stripe	1,240	0.00%	0.00%	99.84%

existing method could not detect lane marks in the liquid stripe images due to a halo that resulted from the sun shining into the camera lens, as shown in Figure 5. Of course, some very stubborn cases were still undetectable by the proposed method, as shown in Figure 17.

6. **Conclusion.** In this paper, we have proposed a versatile LDW system based on 3D visual geometry to prevent drivers' unintended departure from their current lane. The proposed system possesses several special and unique properties that are not present in other existing methods and systems. These properties include the follows: (*i*) The system needs no thresholding to extract lane-mark edges, (*ii*) it can adapt to various weather conditions, (*iii*) it can tolerate the shadow effect, (*iv*) it can reduce the influence of partially covered lane marks, (*v*) it can tolerate low-quality road surfaces, (*vi*) it can tolerate a missing lane mark, and (*vii*) it includes accurate lane departure rather than a rough estimation from the 2D relationship of the lane marks on the images. Based on various images of weather conditions and road surface situations, we examined the effect and efficiency of the proposed system and compared it with other existing methods. With the proposed methods and rectification process, the detection rate substantially increased with a little extra processing time; moreover, the experiments demonstrated that the

proposed LDW system showed excellent results. Of course, a few very stubborn cases were still undetectable, and these will become targets for further research.

Acknowledgment. This work is partially funded by the National Science Council (*NSC*), Taiwan under the grant of the research project *NSC* 97-2221-*E*-008-073-*MY*3.

REFERENCES

[1] National highway traffic safety administration, *Fatality Analysis Reporting System Encyclopedia*, http://www-fars.nhtsa.dot.gov/.

[2] M. Bertozzi and A. Broggi, GOLD: A parallel real-time stereo vision system for generic obstacle and lane detection, *IEEE Trans. Image Processing*, vol.7, no.1, pp.62-81, 1998.

[3] A. Broggi, M. Bertozzi, A. Fascioli, C. G. Lo Bianco and A. Piazzi, Visual perception of obstacles and vehicles for platooning, *IEEE Trans. Intelligent Transportation Systems*, vol.1, pp.164-176, 2000.

[4] Y. Shu and Z. Tan, Vision based lane detection in autonomous vehicle, *Proc. of the 5th World Congress on Intelligent Control and Automation*, Hangzhou, China, pp.5258-5260, 2004.

[5] J. W. Park, J. W. Lee and K. Y. Jhang, A lane-curve detection based on an LCF, *Pattern Recognition Letters*, vol.24, no.14, pp.2301-2313, 2003.

[6] Q. Li, N. Zheng and H. Cheng, Springrobot: A prototype autonomous vehicle and its algorithms for lane detection, *IEEE Trans. Intelligent Transportation Systems*, vol.5, no.4, pp.300-308, 2004.

[7] C. R. Jung and C. R. Kelber, Lane following and lane departure using a linear-parabolic model, *Image and Vision Computing*, vol.23, no.13, pp.1192-1202, 2005.

[8] Y. Zhou, R. Xu, X. F. Hu and Q. T. Ye, A lane departure warning system based on virtual lane boundary, *Jour. Information Science and Engineering*, vol.24, no.1, pp.293-305, 2008.

[9] P. Y. Hsiao, C. W. Yeh, S. S. Huang and L. C. Fu, A portable vision-based real-time lane departure warning system: Day and night, *IEEE Trans. Vehicular Technology*, vol.58, no.4, pp.2089-2094, 2009.

[10] B. R. Chang, C.-P. Young and H. F. Tsai, Simulation and implementation of high-performance collision warning system for motor vehicle safety using embedded ANFIS prediction, *International Journal Innovative Computing, Information and Control*, vol.5, no.10(B), pp.3415-3430, 2009.

[11] C.-P. Young, B.-R. Chang, H.-F. Tsai, R.-Y. Fang and J.-J. Lin, Vehicle collision avoidance system using embedded hybrid intelligent prediction based on vision/GPS sensing, *International Journal Innovative Computing, Information and Control*, vol.5, no.12(A), pp.4453-4468, 2009.

[12] C.-J. Chen, H.-Y. Peng, B.-F. Wu and Y.-H. Chen, A real-time driving assistance and surveillance system, *Jour. Information Science and Engineering*, vol.25, no.5, pp.1501-1523, 2009.

[13] Federal Motor Carrier Safety Administration, *Lane Departure Warning Systems (LDWS)*, http://www.fmcsa.dot.gov/facts-research/research-technology/report/lane-departure-warning-systems.htm, 2005.

[14] Federal Motor Carrier Safety Administration, *Commercial Motor Vehicle Safety and Security Systems Technology Lane Departure Warning Systems*, http://www.fmcsa.dot.gov/facts-research/systems-technology/product-guides/lane-departure.htm.

[15] R. Bishop, *Intelligent Vehicle Technology and Trends*, Artech House, Boston, MA, USA, 2005.

[16] Mobileye Inc., *Mobileye Lane Departure Warning (LDW)*, http://www.mobileye.com/technology/applications/lane-detection/lane-departure-warning.

[17] S. E. Palmer, *Vision Science: Photons to Phenomenology*, The MIT Press, Cambridge, MA, USA, 1999.

[18] D.-C. Tseng, *Monocular Computer Vision Aided Road Vehicle Driving for Safety*, U.S. Patent, No.6765480, 2004.

[19] D.-C. Tseng and Z. Chen, Computing location and orientation of polyhedral surfaces using a laser-based vision system, *IEEE Trans. Robotics and Automation*, vol.7, no.6, pp.842-848, 1991.